Aerospace Science and Technology 172 (2026) 111681

Contents lists available at ScienceDirect

Aerospace Science and Technology

journal homepage: www.elsevier.com/locate/aescte

Hardware-based electric drive train fault detection unit enabling fail-operational capabilities for aviation applications

Leonard Kuhn [a,*], Markus Meindl [b], Christian Bentheimer [a], Martin März [c]

[a] Department of Power Electronics, Group Aviation Electronics, Fraunhofer Institute for Integrated Systems and Device Technology IISB, Schottkystraße 10, Erlangen, 91052, Bavaria, Germany

[b] Department of Power Electronics, Group Energy and fuel cell systems, Fraunhofer Institute for Integrated Systems and Device Technology IISB, Schottkystraße 10, Erlangen, 91052, Bavaria, Germany

[c] Chair of Power Electronics, Department of Electrical Engineering, Electronics and Information Technology at Friedrich-Alexander-University Erlangen-Nürnberg (FAU), Fürther Straße 248 / Fürther Straße 250, Nürnberg, 90429, Bavaria, Germany

ARTICLE INFO

Communicated by Dr Zhang Tao

Keywords:
Fail-operational capabilities
Fault detection device
Hardware-based
Motor drive unit
Aviation application
Pyrofuse

ABSTRACT

The aircraft electrification process imposes safety requirements to ensure the reliability and availability of the electric drive train. Integrating multiple three-phase structures in the motor and inverter is a possible solution to meet these prerequisites. A critical condition to successfully implement such multiple three-phase structures is the ability to isolate faulty subsystems effectively from the overall system. The usage of traditional melting fuses is limited due to possible low short-circuit currents, as they cannot guarantee reliable isolation in such a case. A solution is the use of an active fuse in the DC link of the drive train. For the actuation of such an active fuse, a system is required that detects possible faults in the electrical drive train. This leads to a hardware-based electric fault detection unit (FDU). Therefore, this work aims to develop and simulative evaluate a redundant hardware-based FDU for an active fuse, in this case, a pyrofuse. A new solution that closed the gap in large scale electric propulsion aircrafts fault management concepts.

1. Introduction

New electric motor drive unit topologies based on multiple three-phase structures emerge in the aviation industry to enable fail-operation capabilities of the electric drive train [1]. [1] That structure has been able to reduce the power reductions or even failures of the entire system due to faults, and therefore met the critical prerequisites of reliability and availability [2,3]. The fail-operational capabilities have been only accessible with the functionality to isolate faults within components and subsystems of the aircraft's drive train [3–6]. That prerequisite in the new structured drive trains with an increased level of dependence has required a new fault management and detection concept [6]. A new solution that closed the gap in large scale electric propulsion aircrafts fault management concepts [6].

The classical isolation concept has been a melting fuse, which in that case, could not ensure a correct or reliable isolation due to possible low current faults and no fuse activating in the fault-free subsystems due to the emerging high currents during compensation processes [4,7]. Even in high-current fault cases, reliable passive fuse tripping has been possible only by deactivating the semiconductor short-circuit detection circuit [4].

Further, the isolation time was strongly dependent on the fault current, complicating the ensured functionality of the system during and after the fault due to unpredictable behavior [4,7,8]. To avoid the false tipping of a passive fuse element, the current rating had to be greater than all possible operational occurring current profiles, while ignoring the current direction [4,8]. Power sources capable of only one-directional power flow, such as Fuel cells, have been unaddressed to improve the protection of sensitive sub-components.

These facts had led to an approach with an active fuse. Active fuses are, for example, pyrofuses or pyroswitches. Pyroswitches, in comparison to a pyrofuse, do not disconnect the current, instead, they switch

* Corresponding author.
E-mail address: leonard.kuhn@iisb.fraunhofer.de (L. Kuhn).

[1] Also part of the Bavarian Aviation Research Program BayLu25 under the project of BLU-2109-0014 HeDrive - vollelektrischer Antriebsstrang für Hubschrauber. Additionally in the HORIZON-JU-Clean-Aviation Program managed through EU Funding under the project 101101967 NEWBORN - NExt generation high poWer fuel cells for airBORNe applications.

https://doi.org/10.1016/j.ast.2026.111681
Received 12 August 2025; Received in revised form 13 December 2025; Accepted 9 January 2026
Available online 12 January 2026
1270-9638/© 2026 The Authors. Published by Elsevier Masson SAS. This is an open access article under the CC BY license (http://creativecommons.org/licenses/by/4.0/).

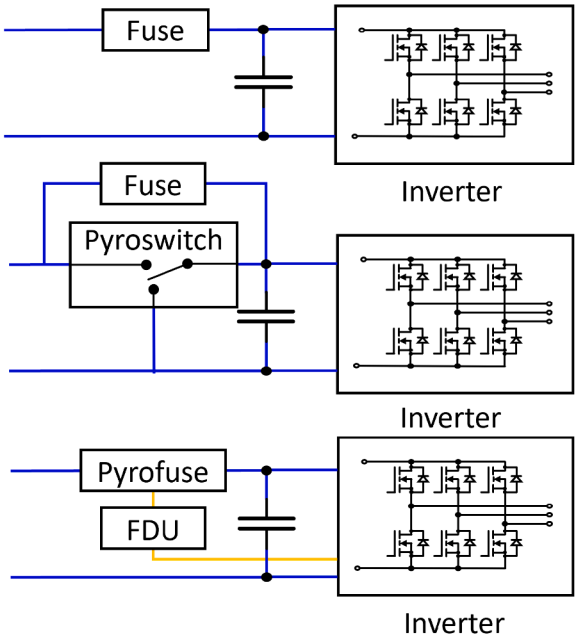


Fig. 1. Illustration of different isolation methods with different fuses.

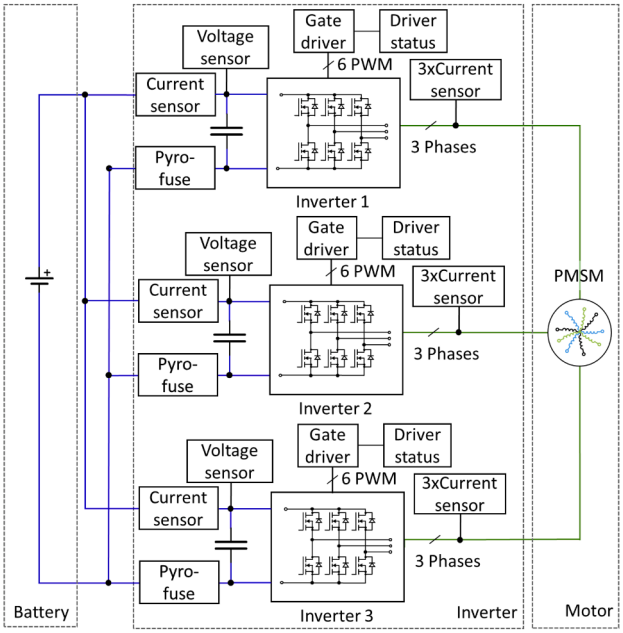


Fig. 2. Overview of the investigated electric drive train.

the current to another path with a passive fuse, while decreasing the conductive losses during the normal operational working state [9–13]. The Pyroswitch could only achieve reliable passive fuse tripping through connecting the faulty path with the other potential [9]. Therefore, reliably high fault current through a passive fuse was generated, and hence a fast isolation of a faulty subsystem was possible [9]. This enabled the functional capability of a passive fuse, while the short-circuit detection of the semiconductors was still activated [4,9].

However, switching an active short circuit is linked to many risks and influences on the electrical drive train and was therefore unacceptable. The current development of pyrofuses made it possible to disconnect the fault current by the activation of a Pyrofuse without the use of a classic fuse while reaching nominal operating voltages greater than 1000V and currents of up to 1000A, making pyrofuses suitable for the megawatt scale [6,7,11]. Other advantages of pyrofuses are lower conductive losses and shorter, quicker, and more consistent fault-clearing time compared to a melting fuse [10].

The three mentioned types of Fuses, melting Fuse, Pyroswitch, and Pyrofuse, are illustrated in Fig. 1 within such a multi-phase motor drive train.

With an active fuse, a trigger signal for activation is required, illustrated as a yellow signal line. Such a trigger signal has to be generated when a faulty condition has been detected, which requires the isolation of one or more components. In typical applications, like the automotive industry, these trigger signals can be generated with an external trigger signal [9–12], a local current sensor [14], or self-triggered [11,13]. The existing protection gap of conventional fuses for low current faults has been closed with the trigger signal [11].

The self-tripping approach was implemented using a smaller fuse, which is unable to disconnect the expected short-circuit current [13]. In the event of an overcurrent fault, the fuse's low ohmic isolation resistance conducts the current through the ignition circuit of the pyrofuse [13]. Most of the problems of a classic fuse approach have remained. The handling of complex error scenarios remained unsolved. The main advantage of this approach was the reduction in conductive losses compared with a melting fuse [10,12,13].

There have been solutions using a local current sensor in a hardware-based approach. As these provide only one decision criterion, these solutions could only detect overcurrent faults. As a consequence, these have been well suited to protect the main battery in such a drive train, but not loads within this drive train. To isolate faulty elements in a fail-operation capable electric drive train, an adapted fault management concept was needed due to the complex fault scenarios. These scenarios generate high equalizing currents in fault-free systems, which would have led to faulty trigger signals, as these would be recognized as overcurrent faults. An illustration of these currents is presented and described in Fig. 5 [14].

Therefore, only an externally generated trigger signal, which includes multiple sensor inputs, can enable situation-dependent ignition. An infeasible way of implementation in the aviation industry is software-based. The certification of a software-based approach in such safety-critical applications is too time-consuming and complicated, as the expected effects of this circuit range from major to hazardous [15].

One possible solution to simplify the certification process is a hardware-based approach. This approach is presented in this work and needs to detect fault conditions that require the isolation of a faulty subsystem.

For this purpose, a drive train consisting of three independent three-phase motor structures was investigated. No existing publication provided a hardware-based method capable of reliably detecting fault scenarios in complex, multi-structured electric drive systems and generating the corresponding trigger signals required for fail-operational behaviour. This gives the developed system the capability to handle faults and, with that, meet the prerequisite of fail-operation capabilities.

2. Overview of the investigated electric drive train and the resulting fault scenarios

The general Structure of the considered drive train is shown in Fig. 2.

It can be seen that one battery provides the total energy of the system, which is connected to three independent subsystems via one main DC link cable. Each of these subsystems provides three phases of the nine motor phases. The motor topology used is a surface-mounted permanent magnet synchronous motor (PMSM), with three isolated winding systems, each three phases are in a star connection. The star points of the three winding systems are isolated against ground. The winding systems are additionally isolated from each other. This enables independent and to other subsystems separated power generation.

Each of the subsystems consists of a DC link capacitor, a B6 bridge inverter with independent sensors, gate drivers, and one pyrofuse. In this work, a subsystem can be understood as an independent motor drive unit with its own electric motor. Due to the physical short distance and low ohmic connections between the DC link capacitors, failure currents are propagated through the DC links between these subsystems. The design of the motor winding system corresponds to a separated structure, which leads to a significantly reduced mutual inductance between the subsystems. Nevertheless, there is a strong magnetic coupling between the phases within a subsystem. This magnetic coupling in a subsystem differs for the three phases. The three phases of a subsystem are referred to as U, V, and W. The naming is identical for each of the three parallel systems in the folllowing. The mutual induction between the outer windings U and W of one subsystem named (MUW) is lower compared to the mutual induction (MUV, MVW) of the neighbouring windings. The subsystems are identical, which leads to the same mutual inductance, within the individual subsystems. However, the asymmetry of the mutual inductances was neglected in the development of the model, as the sum of the self-and mutual inductances in the d- q- system is constant. This behavior is relevant during a fault, as it influences the back electromotive force (BEMF) of the motor [16].

To simplify the fault simulation, a constant inductance value was used. Additionally, no demagnetization occurs during the fault, simplifying fault system reactions. Finite element analysis allows for a more accurate determination of system responses and the non-linear behavior. However, this primarily influences the magnitude of the results, which enables this simplification for these investigations. Demagnetization is considered in detail in publications [17,18].

One of the key factors in this approach are the sensor characteristics. It is common in the aviation industry to use an increased number of sensors to meet the high safety requirements, which enable and simplify the technical detection of faults via hardware. With their corresponding location, these sensors are shown in Fig. 2. Each subsystem has a DC voltage measurement at the DC link capacitor and a DC current measurement before the capacitor. The DC current sensor is located on the high-potential side, while the pyrofuse is located on the low-potential side of the DC link connection of each subsystem. Accordingly, the peak fault currents differentiate from the current through the pyrofuse. In addition, each of the motor phase currents is monitored. The status signals provided by the gate drivers include one error signal for each power semiconductor. This error signal is, for example caused by the DESAT protection. Within the driver, these are referred to as high-side (FLTHS) and low-side (FLTLS) output error.

An overview of possible faults that appear in this electric subsystems is given in Table 1. Faults can emerge within every drive train component including the PMSM, the inverter, and the sensor system. Also, different emergency operating scenarios should not lead to an activation of a pyrofuse, and therefore, these scenarios must be considered. It is also possible to further differentiate between symmetrical and asymmetrical faults. In the case of a symmetrical fault, the influence on the three motor phases of one winding subsystem is equal [19]. This is not the case with asymmetrical faults [18,20].

There are multiple papers analyzing the possible faults within the electric drive train. The three symmetrical short circuit faults are well investigated in [19]. The short circuit faults of the DC link capacitor and the half-bridge differ only in the fault positions but are within the same electrical potential. The three short-circuited motor phases of one subsystem differ only in the current sensor signals of the motor phases in comparison to the other symmetrical short-circuit faults. The difference is caused by the location of the motor phase current sensors within the short-circuit path. The motor phase currents within the motor, the DC link voltages, and the short-circuit current are almost identical for the different symmetrical faults. The effects of these faults on the electrical drive train are so significant that it is necessary to trigger the pyrofuse and isolate the faulty subsystem. This is marked in a separate column for all faults in Table 1.

Table 1
Considered faults in an electric drive train that consists of 3 independent subsystems.

Type of fault	Reference source	Fuse activation
DC link capacitor short circuit	[19,21]	✔
Half bridge short circuit	[19]	✔
Three motorphases short circuit	[19]	✔
One lower switch short circuit	[18,20]	✔
One upper switch short circuit	[18,20]	✔
Two motorphases short circuit	[18,22]	✔
Inter-turn short circuit	[23–25]	✘
Short between two subsystems	[25]	✔
DC link capacitor open circuit	[21]	✘
Half bridge open circuit	[26]	✘
One lower switch open circuit		✘
One upper switch open circuit		✘
One motorphase open	[26,27]	✘
Two motorphases open	[27]	✘
Three motorphases open	[27]	✘
Demagnetization	[18,27]	✘
Sensor fault	[5,28]	✘
Operation with two of three subsystems		✘

The asymmetrical shorts are presented in [18]. Asymmetrical faults can lead to significantly higher fault currents within the motor and can therefore lead to greater demagnetization and with that, to a more significant destruction of the motor compared with symmetrical short circuit faults. This is particularly relevant in the context of fail-operation capabilities to protect the power generation of the other subsystems, and the reason for the required isolation of the faulty system.

The inter-turn short circuit fault is a fault between the two turns of one stator phase. It is the most common fault within the motor windings [24]. The short-circuit current induced by the back EMF leads to rapid propagation of the fault due to the high current. The cause of the propagating character is uncontrolled local thermal overloads, which can lead to demagnetization of the magnets [24]. Detection of the fault is only useful at an early stage of the fault, when there is still a chance of avoiding damage to the entire phase or winding [5]. After successful detection, the control system can reduce the flowing short-circuit currents by taking suitable countermeasures, such as switching an active short circuit by connecting all phases on one voltage potential or weakening the field. This was analyzed in detail in [24]. Disconnection should only take place when the winding short-circuit fault has degenerated into a short-circuit fault between two or more motor phases [5,27]. This is marked accordingly in Table 1.

Short-circuit faults between phases of different subsystems are a special phenomenon of multiple three-phase structures. The reason for this is the physical overlapping of different winding systems at critical points within the used motor. This possible fault leads to complex fault current behaviors and fault detection methods. One of the most important aspects of this error is the current that flows between the two subsystems, leading to a complex phase-dependent fault current. These fault requires the isolation of both faulty subsystems.

Open Circuit faults are another category that had been investigated during this work [21,26,27]. These faults have in common that the fuse in the affected subsystem does not trip, as shown in Table 1. The effects of open-circuit faults are significantly lower than those of short-circuit faults. In this work, these faults were simulated by open switches or not activated MOSFETs. As the influence of these errors is limited and no fault detection is required, the results of the analysis are not discussed in detail.

Other faults, such as ground faults from the AC or DC side, would not lead directly to a fault current, as the system is built up as an IT system with all high-voltage parts and connections isolated against ground. With this, a ground fault does not require a fuse activation. Demagnetization and mechanical loss of magnets are other possible faults.

Mechanical faults have not been taken into account further for this analysis. This includes air-gap irregularities caused by rotor eccentricity or bearing failures.

In addition, sensor faults can lead to incorrect fault detection's and thus may cause a false triggering. For this reason, the sensor values should be monitored. A possible solution to monitor sensor faults is described [28].

3. Fault detection unit

The developed FDU is a modular developed unit, individual working for each subsystem. This leads to one FDU per subsystem, with the possibility of adapting to every number of multiple three-phase structures. Every unit detects faults that require the activation of the pyrofuse. The FDU is therefore the link between the incoming sensor signals and the activation circuit of the fuse.

There are many ways to detect errors, while incorrect fuse activation must be avoided. The traditional melting fuse current rating is conditioned by the I^2t curve, which determines the energy introduced into the fuse [4,8]. However, this method had the disadvantage of a detection time delay depending on the magnitude of the current, kept the potential protection gap, and further did not take into account the direction of the fault current [11]. In addition, high equalizing currents could have led to false detection due to the complex structure of multiple connected subsystems. The solution presented in this work uses different fault indicators (FI) to prevent possible fault detection. One reason for potential fault detection could be a sensor signal fault, which can be monitored externally. The presented solution ensures correct behavior through the use of at least two FIs, passing over single FI faults.

The input signals of the FDU are the sensor values provided within each subsystem. These sensor signals can be differentially or superimposed with noise. The resulting filter cutoff frequency uses the expected noise and the performance capabilities of the sensors as references. That reduces the reduction of the sensor bandwidth and minimizes the reaction time of the FDU. The FDU works in the time domain. Therefore, a signal transformation is unnecessary. Every input signal is analyzed and can lead to an FI if the sensor values are above a certain threshold. The threshold can be adapted to the requirements of the corresponding systems, leading to an FDU that is widely compatible with different drive trains. The generated FIs are then used to diagnose specific faults, which can lead to an activation signal for the fuse. The core of the FDU is the diagnosing process. The approach shown in this paper is in an analog manner.

3.1. FDU logic

Fig. 3 shows the detection logic developed in this work, which presents the core of the FDU.

The circuit consists of two parallel, similar logic paths, each performing fault detection. The upper circuit detects faults that lead to the required isolation of a faulty subsystem, except short-circuit faults between two subsystems. The lower circuit is specially designed for the detection of faults between two subsystems and is described separately due to small but relevant differences.

The distinction between the upper and the lower circuit in Fig. 3 is made by checking whether the sum of the motor currents in the monitored subsystem is equal to zero. A summing amplifier is used for this purpose, including a certain threshold to generate the corresponding FI. The measurement accuracy of the sensors used and the desired responsiveness of the developed FDU influence the threshold. In a final logical AND element, the upper circuit is blocked if the sum of the currents is not equal to zero. At the same time, the lower circuit is activated. This separation is necessary due to different fault current behaviors, which are analyzed in Section 3.2 for faults between two subsystems. It is also relevant that a faulty summing current can only be detected if all phase current sensors are within their measuring range and not saturated. In the event of a fault, this can quickly become the case. Therefore, the detection of this FI is blocked if a phase current exceeds its measuring range. To ensure a correct time-delayed error detection, the detection of this FI is stored for a certain period within a latch. The latch update frequency is negligibly low. In addition, this FI is periodically detectable in the event of a short circuit between two subsystems.

On further investigation of the upper circuit, which is responsible for all faults that appear within one subsystem, three different combined FIs cause the activation of the pyrofuse. Two of the FIs are higher in priority. The sum error of the motor currents, and the positive DC current. While the sum of the motor currents detects whether the fault only affects one subsystem, the DC current FI prevents a fuse activation without a certain fault current. In the event of faults within one subsystem, only a positive DC fault current can occur, which indicates a fault in the corresponding system. This current leads to discharge currents in the other subsystems. These are appearing as negative DC currents, while a fault influences another subsystem. The negative currents are usually supplied by the DC link capacitors of the individual subsystems. This detection method helps to prevent false detection of equalizing currents as overcurrent faults.

The overcurrent events in the motor phases must exceed predefined thresholds to generate an FI. These thresholds exists for positive and negative current values. The voltage related FI is further divided into a minimum limit of the DC link voltage and a derivative element that recognizes voltage changes over time. The voltage limit can be triggered by the dip in the DC link voltage, which occurs while large short-circuit currents flow. The derivation of the DC link voltage is a time-dependent control mechanism. The threshold for an absolute value is required to be defensive to ensure no fault detection in fault-free subsystems, the derivation can be more sensitive. With this method a fast decrease in the DC link voltage can be detected, as appears with a short circuit, with this method.

Identification of increasing voltages is also possible, which can be the result of inrush currents. This is a great advantage in the complex fault and fault clearing behavior in the analysed system. In a fault-free subsystem, the inflow of current should lead to an increase in the measured voltage. Therefore, the expected derivation result will be positive. For a fault within a subsystem, the increasing current will not lead to a voltage increase, because the current increase is caused by a voltage dip.

The time delay of the different sensors must be taken into account. Correct fault detection is only possible if current and voltage are detected synchronously. An additional trigger suppression for a few microseconds can simplify this time synchronization.

The lower circuit handles short circuit faults that can appear between two subsystems. This circuit has many similarities with the upper circuit. It differs in the following points. First, this circuit has two instead of one way to generate an ignition signal. The first option requires only two FIs. An overcurrent detected by the DC current sensor and the FI for the summing phase currents unequal to zero. This is needed, due to the active DESAT fault handling, which can prevent the occurrence of additional FIs simultaneously. Disconnection therefore occurs when positive fuse currents are detected and the sum currents are not equal to zero. Nevertheless, from the identification of two independent FIs, redundancy is warranted. In addition, equalizing currents are within the operating current range in the case of a fault between two subsystems, leading to no inrush current detection reaching the corresponding threshold.

The other combination that can lead to an activation signal is the occurrence of negative DC currents. The negative residual current only leads to tripping when further FI signals are detected. This is important because negative fuse currents usually occur in fault-free subsystems, except for faults between two subsystems. This FI is included for faults between two subsystems since it can decrease the detection time. The expected possible maximal time delay by ignoring negative fault currents is 1ms, which is not tolerable. The resulting fault currents are further described in Section 3.2.3.

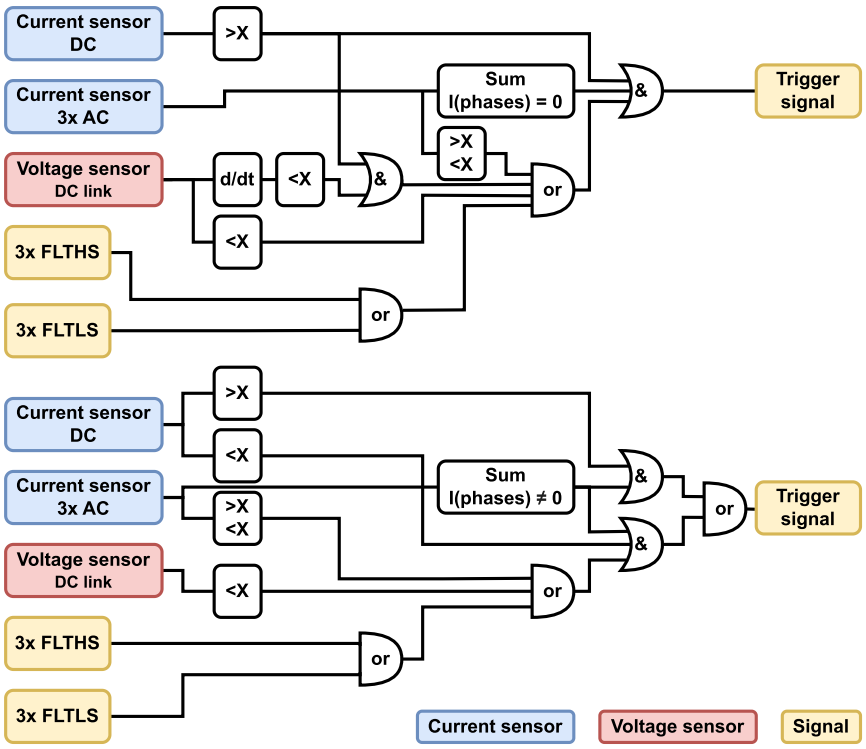


Fig. 3. Functional block diagram of the developed FDU logic.

Another significant change is that the time-dependent FI of the DC link voltage is excluded. The voltage changes are less significant in amplitude for this fault, which makes reliable detection unnecessarily difficult due to the necessary threshold adaptation. In addition, it is expected that the time-dependency of positive and negative fault currents between the two subsystems, which are influencing the DC link voltage, is mostly driven by the semiconductor drivers. Overall, both subsystem's semiconductor drivers are influencing the fault currents and with that the DC link voltage changes. This cross-correlation makes the FI generation difficult to assign correctly. The minimum voltage value is a redundant extension, to keep the ability to detect other serious faults, with the compromise of a possible longer recognition time.

The other FIs include the detection of DESAT faults, the detection of overcurrent events in the motor phases, and the detection of FIs corresponding to the DC link voltage. These lower-priority FIs are adding redundancy within the FDU. Two FIs are always required to generate an ignition signal.

In this proposed variant of the detection circuit, no distinction of the fault location is made within the subsystem for a fault between two subsystems. Due to the radial arrangement of the phase systems to each other, faults can only occur between one subsystem at the terminal point of the winding system and in the other subsystem at the neutral point. However, this only applies to the motor design presented here.

Such a distinction is possible and would enable selective disconnection behavior, and can therefore save possible additional power in the drive train. A distinction of the fault location is made by checking whether an increase for the phase current occurs in one or more than one phase within one subsystem. This differentiation was not pursued further in this case, as ignition of the fuses in both subsystems is desired. This is due to the fact that it is not possible to suppress the residual currents between the subsystems if only one pyrofuse is triggered. This also applies if the control system actively intervenes. In addition, the control system still needs to intervene when the pyrofuse is triggered in both subsystems in the investigated power train.

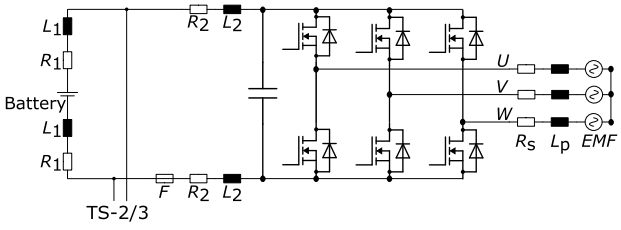


Fig. 4. Overview of one subsystem equivalent circuit in LTspice.

3.2. FDU verification process

The verification process of the FDU was carried out using simulations. All investigated error scenarios are summarized in Table 1. The focus of this work is to demonstrate the working mechanism of the developed FDU logic. The two most relevant faults are presented in this section. First, the DC link capacitor short-circuit fault and second, the short-circuit fault between two subsystems are presented. Both faults are shown without active DESAT fault handling of the semiconductor bridges. Functionality has been analytically confirmed even with an active DESAT treatment.

3.2.1. Fault simulation setup

The software used for the simulation is LTspice. The simulation model essentially corresponds with the model shown in Fig. 2. In Fig. 4, one of three subsystems is displayed. Three of these equivalent circuit models are connected in parallel for the fault analyses, symbolized by *TS-2* and *TS-3*.

The resistance and inductance of the supply line and return wire of the battery cable are simulated by R_1 with 1.5mω and L_1 with 500nH.

Table 2
Main parameters of the drive train.

Drive train parameter	Value
DC link capacitor nominal voltage	$V_C = 800\,\mathrm{V}$
DC link subsystem capacitor	$C = 180\,\mu\mathrm{F}$
DC subsystem nominal current	$I_C = 312\,\mathrm{A}$
Phase current	$\hat{i}_P = 500\,\mathrm{A}$
Stator current frequency	$f_s = 956\,\mathrm{Hz}$
Stator resistance	$R_s = 2.8\,\mathrm{m\Omega}$
$d-q-axis$ stator inductance	$L_d = L_q = 75.8\,\mu\mathrm{H}$
Stator inductance	$L_s = L_d = L_q$
Permanent-magnet flux linkage	$\psi_{pm} = 55.511\,\mathrm{mVs}$

The resistance and inductance of the busbar within the inverter for one subsystem are simulated by R_2 with 10mω and L_2 with 20nH.

F shows the location of the fuse, in this case, the active fuse element or pyrofuse. The battery has an internal resistance of 18 mΩ and an inductance of 1 µH. The DC link capacitor is located before the B6 bridge inverter topology, followed by the PMSM. Each subsystem capacitor has an equivalent series resistance of 20 mΩ and a capacity of 180 µF. An LR-circuit simulates the short circuit with an inductivity of 15 nH and a resistance of 1 mΩ.

The active fuse isolation process is subdivided into three time segments. The first segment is the time between the fault and the detection of the fault. This time is based on the fault characteristics. Due to the complex structure of the drive train as a multiphase system, the FDU is also inversely dependent on the other two time segments. The second segment is the delay between the detection of a fault and the beginning of the fault isolation. During this segment, the FDU trigger signal leads to fuse ignition. 500 µs are used in this analysis and is a implemented constant delay element. The time delay consists of the communication time, the instructions to trigger the trigger element, and the ignition time. The ignition time is the time the pyroelement within the pyrofuse needs to absorb enough energy to ignite. Throughout this phase, the fault current is not influenced by the fuse, as it still provides normal conducting properties. Due to this, the current can continue to increase, decrease, or fluctuate. The concrete current behavior depends on the fault. This delay is within the 500 µs. Values below 200 µs for this delay element are possible with the selection of different igniters and faster communication speeds with the fuse trigger element. The ignition of the fuse begins the last time segment. This section starts with the beginning of the isolation process and ends when the pyrofuse has completely isolated the faulty subsystem. The duration of the third time segment depends on the fault and the short circuit characteristics. The system experiences compensating processes during this segment that strongly influence the FDU. Therefore, this had be taken into account during the FDU verification.

In this analysis, the first time segment for the detection of a fault takes up 444 µs depending on the fault characteristic, the second time interval is component dependet and constant 500 µs long, the last and third time segment takes up to 1.36 ms and is also fault depending.

The parameters of the drive train are provided in Table 2 for a fault free system at nominal values.

3.2.2. Short-circuit fault in the DC link capacitor

The short-circuit fault in the DC link capacitor is simulated by the described LR circuit, switched in parallel to the capacitor at 1 ms and marked with a vertical dashed line t_{fault}. The resulting fault behavior for the three subsystems is shown in Fig. 5. The DC link current (blue) is measured with the corresponding current sensor, and the voltage (red) is measured at the DC link capacitor for each subsystem.

In the upper graph are the values of the faulty subsystem 1, while in the lower graph the plots for subsystems 2 and 3 are located. As the drive drain subsystems are arranged symmetrically, system 2 and 3 are nearly identical, for faults influencing one subsystem. Therefore only on of the fault-free systems is plotted.

In the event of the fault (t_{fault}), an increase in the fuse current with peak values of up to 15.3 kA can be observed in subsystem 1. This is reached shortly after the fault occurs.

The DC link voltage at the capacitor is now defined by the RL circuit connected in parallel. As this resistance value is significantly lower, a fast discharge of the capacitor takes place. It should be noted that the peak fault current flowing is 29 kA, which is considerably higher than the measured current for the fuse, due to the capacitor discharge. The capacitor voltage reaches a minimum value of 58 V within 30 µs after the fault.

Mathematically, this can be simplified in a first step as the discharge curve of a series RLC circuit. In this circuit, the sum of the voltages is equal to zero, as in

$$v_R(t) + v_L(t) + v_C(t) = 0 \tag{1}$$

The resulting homogeneous second-order differential equation with constant coefficients is shown for the subsystem DC-Link capacitor and the short circuit path in [29].

$$\frac{d^2 v_c(t)}{dt^2} + \frac{R}{L}\frac{d v_c(t)}{dt} + \frac{1}{LC} v_c(t) = 0 \tag{2}$$

The characteristic equation of this is

$$s^2 + 2\delta s + \omega_0^2 = 0 \tag{3}$$

$$s_{1,2} = -\delta \pm \sqrt{\delta^2 - \omega_0^2} \tag{4}$$

$$\delta = \frac{R}{2L}, \qquad \omega_0 = \frac{1}{\sqrt{LC}} \tag{5}$$

The solution for the capacitor voltage of this resonant circuit is then determined, if the series RLC circuit is overdamped or underdamped. The shorted RLC circuit alone reacts as an overdamped circuit with a decay of the transient voltage without oscillation [29].

Due to the very low-resistance DC link connections, large equalizing currents occur between the fault-free subsystems and the faulty one. The currents of the fault-free subsystems are in the opposite direction also discharging it's capacitor. This can be seen between t_{fault} and t_1. The negative equalizing currents from the fault-free subsystems reach values of up to −5.4 kA 10 µs after t_{fault}. Shortly after the discharge, the currents rise to a peak of 0.8 kA at t_1, which is 60 µs after t_{fault}.

The influence of the fault is also visible by the collapse of the DC link voltage, which reaches a minimum of 310 V and then stabilizes at 435 V. The minimum value is present after 30 µs and is caused by the current-driving properties of the parasitic line and fault inductance.

Including the discharge RLC circuits of the other fault-free subsystems and the battery source, the system's response becomes underdamped. The point t_1 is therefore an overshoot of the sudden capacitor discharge.

512 µs after t_{fault} the fuse begins the isolation process. This ignition leads to a sudden change in the voltage that drops over the fuse, introducing very strong balancing currents marked at t_2, with 1.9 kA for each fault-free subsystem. This is again an oscillating response of the charging system.

With t_1 and t_2 two positive current peaks exist, that potentially lead to a false fault detection, introduced by equalization currents. With a decrease in the damping, the expected oscillation will be greater, and with that, potential peaks for false fault detection.

The fault impact is further analyzed in Fig. 6. The DC link voltage and current, phase currents, and the detection signals of the FDU are therefore plotted. The lower graph section shows the trigger signal of the FDU, and in between is the plot for the three-phase currents. With the fault, the phase currents of this subsystem begin to oscillate. In addition, the oscillating phase currents have an offset component that decays over time.

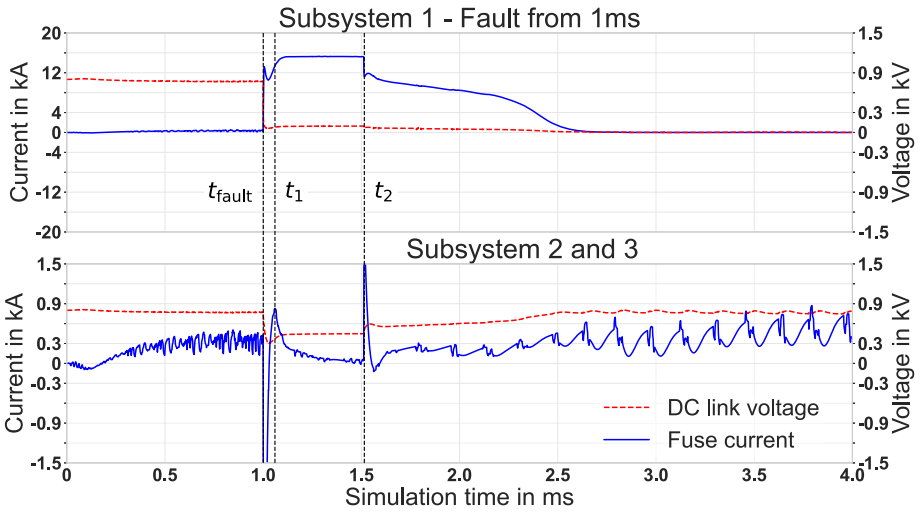


Fig. 5. Measurement signals for the subsystem 1 and subsystem 2 and 3 in the event of a short-circuit fault of the DC link capacitor in subsystem 1 from 1 ms.

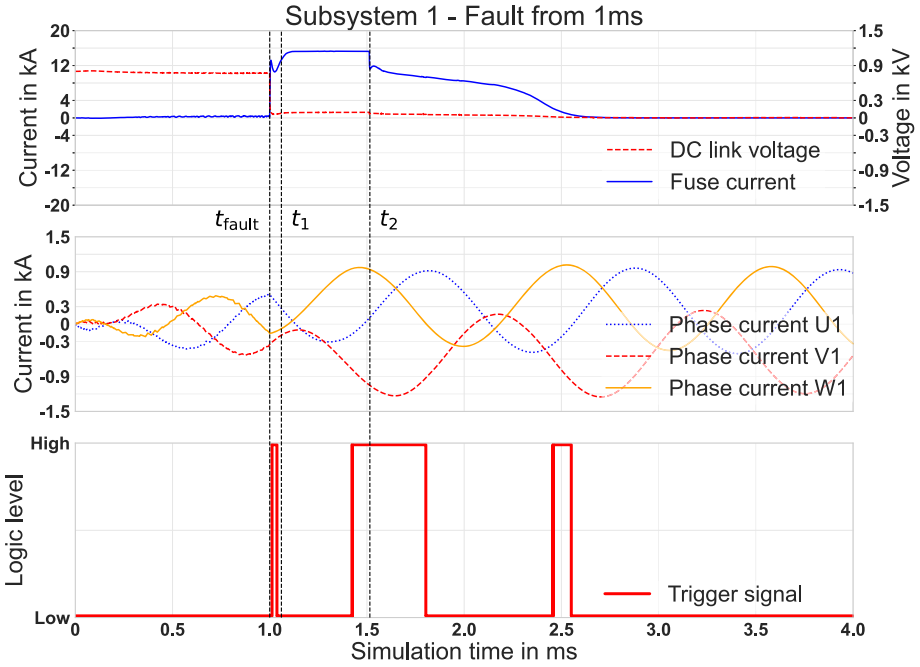


Fig. 6. Measurement signals and output signals of the FDU for the subsystem 1 in the event of a short-circuit fault of the DC link capacitor in subsystem 1 from 1 ms.

Describing them in a steady-state analysis, as in (6), is done under the assumption that the terminal voltages U_d and U_q are equal to zero due to a symmetrical fault. It is assumed that all machine parameters remain constant. Furthermore, it is specified that no demagnetization and no change in rotor speed occur during the fault, and that the terminals were open before the fault. Accordingly, the motor is in a no-load condition prior to the fault [17].

$$\begin{aligned} 0 &= (R_s + sL_d)i_d(s) - \omega_e L_q i_q(s) \\ -\frac{\omega_e \Psi_{pm}}{s} &= (R_s + sL_q)i_q(s) + \omega_e L_d i_d(s) \end{aligned} \tag{6}$$

This Equation can be solved for $i_d(s)$ and $i_q(s)$, and is explained in detail in [17]. Converting these equations for i_d and i_q using the inverse Park transformation yields the phase currents. The result for phase U is calculated in the time frame.

$$\begin{aligned} i_u(t) = &-\frac{\Psi_{pm}}{L_d}\cos(\omega_e t + \alpha) + \\ &\frac{\omega_e \Psi_{pm}}{2} e^{-t/T_a}\left(\frac{1}{\omega_e L_d} + \frac{1}{\omega_e L_q}\right) + \\ &\frac{\omega_e \Psi_{pm}}{2} e^{-t/T_a}\left(\frac{1}{\omega_e L_d} - \frac{1}{\omega_e L_q}\right)\cos(2\omega_e t + \alpha) \end{aligned} \tag{7}$$

The solution consists of three components. The first line, represents the steady-state component, followed by an exponentially decaying offset component in the second line and an exponentially decaying component with twice the frequency in the third line. In some sources, for example in [30], the steady-state component includes a transient and a subtransient part. Both can be neglected for the motor analyzed here. The transient part does not exist because a PMSM has no field winding.

The subtransient component describes coupling effects between the stator and the rotor, which do not exist in the investigated machine

due to the absence of damper windings. In addition, for symmetrical inductances in the d- and q-axes, the component oscillating at twice the electrical angular frequency becomes zero. Thus, only a steady-state component and an offset component that decays with the transient time constant of the armature circuit remain. The parameter α describes the offset of the initial rotor position at time zero [17,30].

In summary, it can be stated that the phase current can reach at most twice the static value. The remaining static offset component peak value equals 732 A, mainly depending on the permanent magnet flux linkage and the motor inductance [17,30]. The decaying offest component is visible in Fig. 6.

The FDU detects the response of this fault a total of three times. For the first time, as early as 11.94 µs after the occurrence of the fault (t_{fault}). The two detected fault conditions are the current through the fuse and the voltage dip in the DC link. The overcurrent event was already detected 60 ns after the fault occurred. This FI is present for the entire uncleared fault duration. The voltage drop was detected after 5.92 µs.

Since this fault is only affecting the circuit in one Subsystem, the sum of the phase currents stays equal to zero. According the presented FDU logic in Fig. 3, this fault is part of the upper logic. In this case, a positive overcurrent FI and a voltage FI are two FIs indicating a fault that leads to the triggering signal. This trigger signal is present for 50 µs, which is more than sufficient to register this fault.

The second trigger signal occurs when the phase currents exceed the defined threshold, that are leading to the corresponding FI. This happens repeatedly between 1.4 ms and 1.8 ms, as well as between 2.45 ms and 2.9 ms. Consequently, the second trigger signal is present 0.4 ms after t_{fault}, and the third trigger signal 1.45 ms after t_{fault}. However, this signal is greatly shortened, as the fault is isolated from 2.6 ms onwards to such an extent that the FI of the fuse current is no longer present.

In conclusion the FDU is therefore able to successfully detect this fault and trigger the fuse, for the faulty subsystem. However, the FDU must ensure that no trigger signal is generated in the fault-free subsystem. Particular attention must be paid to the equalizing currents located at t_1 and t_2. t_1 leads to a voltage increase and with that to the absence of the voltage derivation FI. At t_2 the FIs involved are not directly affected by the start of isolation by the fuse.

The FDU of the fault-free subsystem had to ensure not to generate a false trigger event. The simulation results with the described equalizing currents can be seen in Fig. 7.

The FDU corresponding FI detects the voltage drop. Since this FI is occurring during negative DC currents, it is blocked in the FDU logic. The FI disappears when the DC link voltage is raised with t_1. The currents peak of 0.8 kA at 60 µs after t_{fault}, which already leads to the detection of a positive DC current FI. As the voltage also rises again during this period, this does not lead to a false trigger signal of the fuse due to the redundant fault detection. With the start of the isolation process, high inrush currents exist at the fault-free subsystems, again leading to the detection of the corresponding DC current FI at t_2 with 2.3 kA. Also, in this case, the voltage-related FI is not present during this state as the voltage rises. Conversely, a time offset between the voltage and current signals can lead to false detection. Therefore, the factors influencing the delay between the current and voltage sensors must be analyzed precisely, and both sensors must be synchronized regarding to each other.

This ensures that in the event of a short-circuit fault on the DC link capacitor, the fault is correctly detected in the faulty subsystem and false detection in the fault-free subsystem is prevented. The developed FDU only shows robust error detection when the input signals are correctly synchronized. To prove that this concept works, the derivative of the voltage is compared with the current threshold detection, shown in Fig. 8.

The fault is a time segment of a low-side switch short, as it is the expected worst case for this working principle. Here, the high side switches a low side switch short multiple times. All the faults presented are without active DESAT handling, the fault impact is greater and the results are therefore clearly visible. The functionality was also confirmed with an active DESAT treatment.

The fault appears in subsystem 1 from 1 ms on (t_{fault}), and the graph shows the impacts on subsystem 2 or subsystem 3. With the occurrence of the fault, the differentiator generates an equivalent output voltage peak of 1.3 V for the falling DC link voltage. This is significantly lower than the 3.1 V for the faulty subsystem. However, the fault has a minor dV/dt characteristic due to the more significant parasitic influence. The 1.3 V is sufficient to detect a voltage drop, while the current measured is negative. This comes with a current overshoot, leading to positive equalizing currents higher than the threshold. The same behavior was described for the DC link short in 7. During the shown pulsating curves from 1.25 ms on, if the high side semiconductor switches on, there is a bridge short circuit due to the shorted low side switch. This leads to a voltage drop with negative currents and voltage rises with positive currents. The equalizing currents, therefore, lead to the appropriate behavior of the differentiator.

As the time delay between the voltage and current sensor is properly equalized, the corresponding FIs do not appear at once. However, it is recognizable that a few µs out of synchronization can lead to false recognition. Within normal short-circuit faults, larger errors are allowed. Therefore, the robustness and functionality of the developed FDU is strongly influenced by this synchronization.

This confirms the basic functional principle of the logic developed for the detection circuit, even in time-critical fault environments.
To further increase the robustness of the system, trigger signal pulse suppression should be considered. With a small delay in the microsecond range, sensor synchronization errors are compensated to prevent false detection. A reasonable value for this pulse suppression is 15 µs. As the run-time might differ for other systems, this value can change.

3.2.3. Short circuit fault between two subsystems

Short-circuit faults between phases of different subsystems are a particular characteristic of this design. Since two systems are affected, it is also necessary to isolate two systems to ensure the functionality of the remaining drive drain. An active DESAT fault treatment has a significant influence on the fault behavior, due to the fact that the semiconductors are in the short-circuit path. In the following, the short-circuit fault between the phase U terminal point of subsystem 1 and the star point of subsystem 3 is analyzed for an inactive DESAT fault treatment of the power modules, and the results for subsystem 1 are shown in Fig. 9 and for subsystem 3 in Fig 10.

The system reaction when a fault occurs depends mostly on the phase angle at the fault occurrence. Due to the fault location, the behavior is a special version of an Inter-turn fault, as the windings of subsystem 3 are fully shorted to the terminal of phase U. The fault path is simulated by an inductance of 15nH and a resistance of 1 mΩ.

The terminal point of phase U in subsystem 1 continues to be switched. Therefore, the fault paths of subsystem 3 are duty cycle dependent, connected with the positive or negative DC-link voltage. In the analysis, no angle displacements between the subsystems were included. As the Back-EMF changes for different displacments, an influence on the fault behavior is expected [31].

The inducted voltage in the short-circuit windings is directly related to the speed and the number of the fault coils [25].

$$\begin{aligned} V_{U3f} &= \omega_e \psi_{pm} \sin(\theta) \\ V_{V3f} &= \omega_e \psi_{pm} \sin(\theta - \frac{2}{3}\pi) \\ V_{W3f} &= \omega_e \psi_{pm} \sin(\theta + \frac{2}{3}\pi) \end{aligned} \tag{8}$$

This inducted voltage and short circuit resistance enable currents in the kA range.

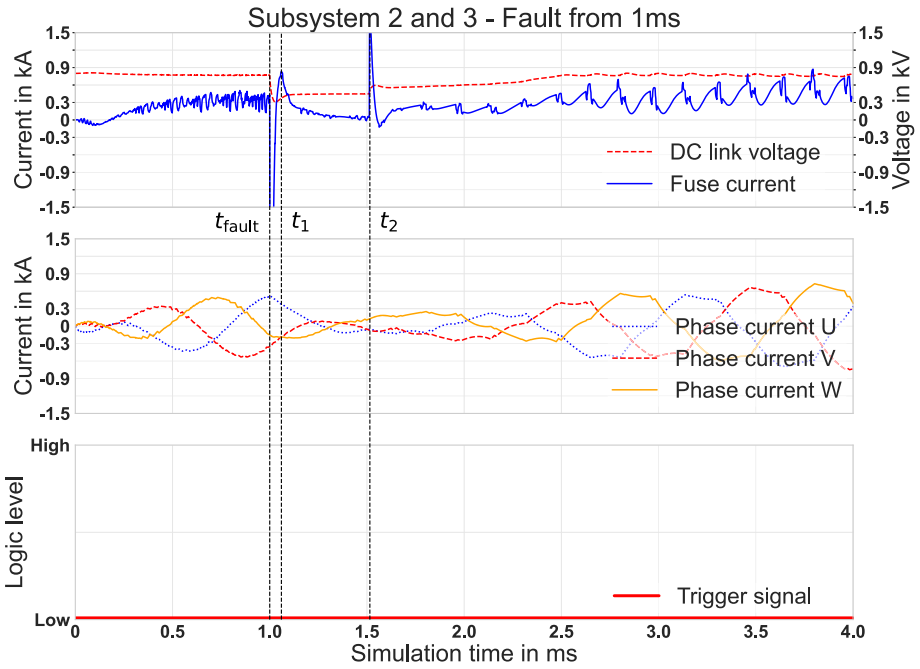


Fig. 7. Measurement signals and output signals of the FDU for the subsystem 2 and 3 in the event of a short-circuit fault of the DC link capacitor in subsystem 1 from 1 ms.

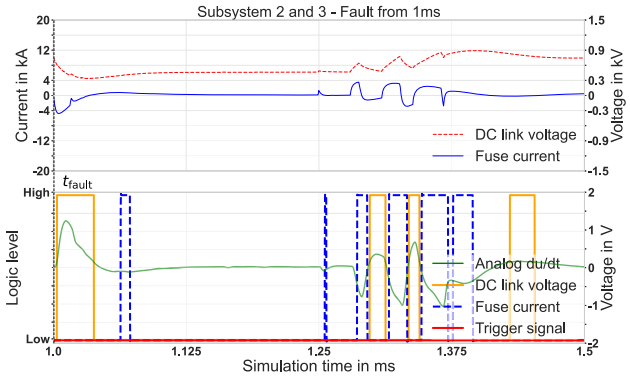


Fig. 8. Measurement signals and output signals of the FDU for the subsystems 2 and 3 in the event of a short-circuit fault in the low side semiconductor in subsystem 1 from 1 ms.

The voltages of the stator windings have to include the short-circuit winding impact, which is therefore included in the matrix elements for the three phases of subsystem 3.

$$\mathbf{V} = R_s \mathbf{i} + L_s \frac{d\mathbf{i}}{dt} + \frac{d\boldsymbol{\Psi}_{\mathbf{pm}}}{dt} \tag{9}$$

These are generating the main drive of the fault currents for the phases in subsystem 3, and are analyzed in [25].

After the fault occurs, the DC link voltage in all subsystems is affected. In addition, the voltage oscillation is stronger and more irregular compared to the other faults from Table 1. The impact of the fault decreases with higher ohmic faults, making voltage-dependent detection difficult.

The DC current also shows a strong fluctuating curve, comparable with a sine, which is superimposed, such as a Fourier series of the second order.

The peak-to-peak value is up to 4.5 kA with a small positive offset, which decreases over time due to a decay of the fluctuating power output. The DC current of subsystem 3 is mainly influenced by the current flowing between the subsystems shown in Fig. 10. It can be described as a sine wave with an amplitude of 2.5 kA. The DC current in the affected subsystem 3 exhibits similar fluctuations as in subsystem 1, but without the superimposition of the first harmonic.

The phase that is short-circuited at the terminal (in this case, phase U of subsystem 1) has a peak-to-peak value of 5.7 kA. In addition, there is a small positive phase shift.

In contrast to that, the effects on phase V and W of subsystem 1 are negligible. The reason for this is that the short-circuit loop does not include phases V and W. The additional current flow in phase U couples with subsystem 3 through the short-circuit path. Therefore, the sum of subsystem phases currents is unequal to zero, which leads to the detection of this FI.

The phase currents experience a strong increase in amplitude due to the induced voltage in the short-circuit windings. The increase in amplitude depends on the phase difference between the conducting phase U in subsystem 1 and the corresponding phase in subsystem 3. The phase W of subsystem 3 is affected the most. All phases in subsystem 3 are facing an increase in the current amplitude.

This causes a trigger signal in Subsystem 3 at 32.2 µs after t_{fault} due to the positive fuse current at t_1, and the FI for the fuse current is detected after 24.2 µs. The phase current fault is detected 30.9 µs after t_{fault}. The relevant FI for a sum current unequal zero occurs after 9 µs and therefore well before the other FIs occur. A DESAT fault detection appears 43.6 µs after t_{fault}. As this FI is after the trigger signal generation, the working principle for an active Desat Fault detection is already proven. Fluctuations in the DC link voltage could also be detected. However, this FI is only present during the maximum amplitude of the DC fault current and is, with that, significantly delayed. Errors in the phase current are detected much earlier in comparison. The derivative of the DC link voltage will be less likely to be detected, with higher fault resistances.

The oscillating fuse current behavior in the first subsystem decreases during the pyrofuse disconnection process and is no longer present after 2.5 ms. However, tripping of both fuses is not sufficient to suppress the fault currents, and thus the residual currents remain. This still requires active intervention of the control system.

In subsystem 3, a trigger signal is generated 444 µs after t_{fault}, which is over 400 µs later than for subsystem 1.

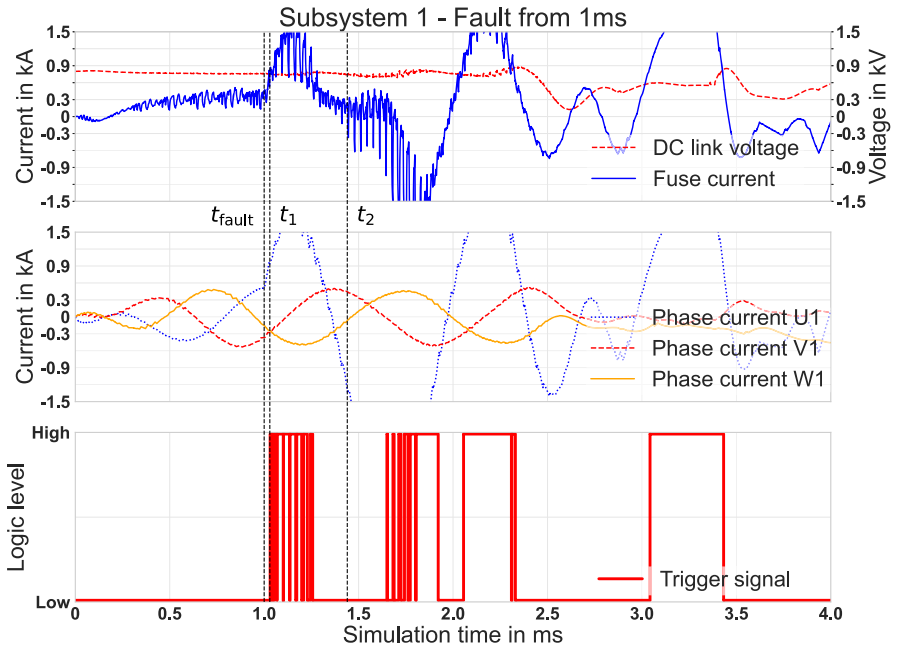


Fig. 9. Measurement signals and output signals of the FDU for the subsystem 1 in the event of a short-circuit fault between the terminal of phase U in subsystem 1 and the star point of the subsystem 3 from 1 ms.

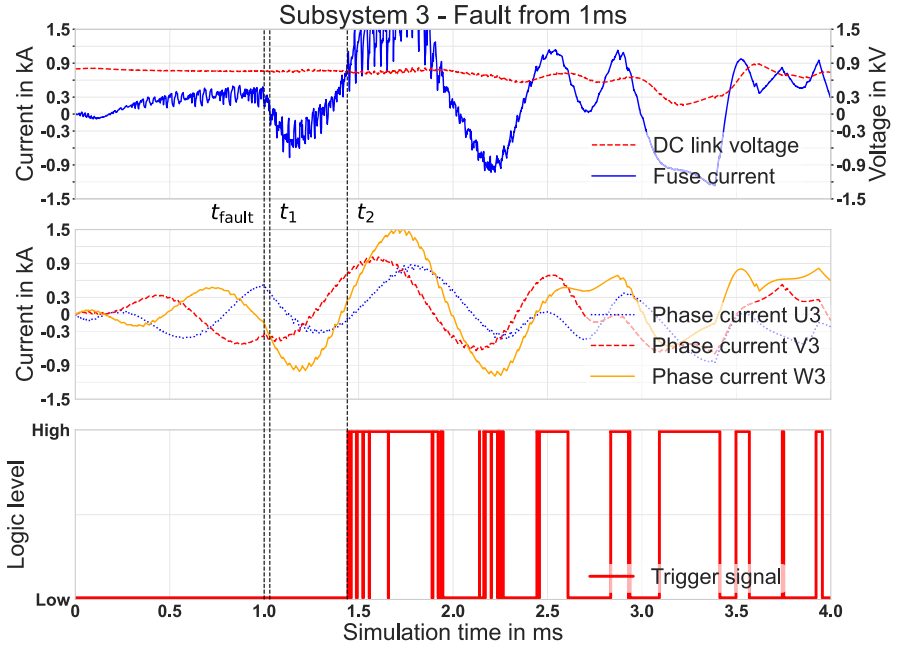


Fig. 10. Measurement signals and output signals of the FDU for the subsystem 3 in the event of a short-circuit fault between the terminal of phase U in subsystem 1 and the star point of the subsystem 3 from 1 ms.

The reason for this delay is that the negative half-wave of the DC current does not reach the threshold value. This is strongly affected by the phase angle present at the time the fault occurs. During this negative half-wave, the phase current FI is identified for the first time at 149 µs after t_{fault} and the DESAT fault at 192 µs. As in subsystem 1, the FI for the sum of the phase currents was detected 9 µs after t_{fault}. The pulsating residual currents decrease with the successful disconnection of subsystem 3. However, significant fluctuations in the fuse current and the DC link voltage remain without intervention by the control system.

A separate investigation with active DESAT fault handling was done for all fault scenarios. It is of great importance for this case, since the fault current-reducing effect can prevent an effective detection. The results showed a trigger signal 32.2 µs after t_{fault} for subsystem 1 and subsystem 3 after 411 µs, with significantly reduced fault currents. The relevant FI for the sum of the phase currents was still detected 9 µs after t_{fault}. The simulation results are shown in Appendix A for subsystem 1 in Fig. A.1 and for subsystem 3 in Fig. A.2.

The results showed that the FDU enables robust trigger generation for faults between two subsystems without compromising reliability. A prototype of this FDU was implemented, supplied with artificial sensor signals. The resulting measurements confirmed the correct and reliable functionality of the FDU.

4. Conclusion

Although widely used, conventional fuses fail to guarantee reliable isolation at low short circuit currents, active fuses do not. This limitation necessitates the use of an active fuse when multiple three-phase structures are employed in the motor and inverter to ensure the reliable isolation of faulty subsystems. In response to this need, a unique hardware-based control system for an active fuse in the DC link of the electric drive train was developed. This system, as a hardware-based FDU, stands out due to its ability to detect potential faults in the electric drive train and generate a trigger signal for the pyrofuse, a feature currently not found for more complex multiphase drive train topologies.

The developed FDU is designed to meet a variety of essential requirements, demonstrating its adaptability. Its modular design allows for adaptation to different numbers of phases, thereby extending its range of possible applications. With a redundant fault detection principle, sensor faults, and possible injecting singles do not lead to false triggering. The necessity to synchronize the measurement signals with individual time delays of the sensors is addressed. Adaptive detection behavior significantly improves the reliability of detecting different faults while taking different load behaviors into account. Additionally, due to the hardware-based processing, the fault detection times are in the low microsecond range at a stator current frequency of about 1 kHz. Total fault clearing times of less than 1.5 ms have been achieved. The rapid behavior of the fuse leads to a strong system reaction with strong equalizing and inrush currents. These currents have been considered, and the time-dependent analysis of the DC link voltage prevents false tripping, instilling confidence in the FDU's reliability.

In conclusion, the FDU's ability to monitor the current as a function of the voltage change is a remarkable advancement. It serves as a high-speed replacement for the I^2t characteristics of traditional fuses, enabling a significantly higher detection speed without compromising on reliability. This efficiency is a testament to the FDU's capability and its potential to revolutionize fault detection in electric drive trains while maintaining requirements for aviation applications and safety.

CRediT authorship contribution statement

Leonard Kuhn: Writing – original draft, Visualization, Validation, Methodology, Investigation, Formal analysis, Software; **Markus Meindl:** Writing – review & editing, Supervision; **Christian Bentheimer:** Writing – review & editing, Supervision; **Martin März:** Writing – review & editing, Supervision.

Declaration of generative AI and AI-assisted technologies in the writing process

During the preparation of this work, the authors used Grammarly and ChatGPT in order to further improve the journal quality. The authors take full responsibility for the content of the publication.

Data availability

Data will be made available on request.

Declaration of competing interest

The authors have declared no conflict of interest.

Acknowledgment

The research was supported by the Bavarian Aviation Research Program BayLu25 under the project of BLU-2109-0014 *HeDrive - vollelektrischer Antriebsstrang für Hubschrauber*. In addition it was also supported by the HORIZON-JU-Clean-Aviation Program managed through EU Funding under the project 101101967 *NEWBORN - NExt generation high poWer fuel cells for airBORNe applications*.

Appendix A. Short circuit fault between two subsystems with active DESAT fault handling.

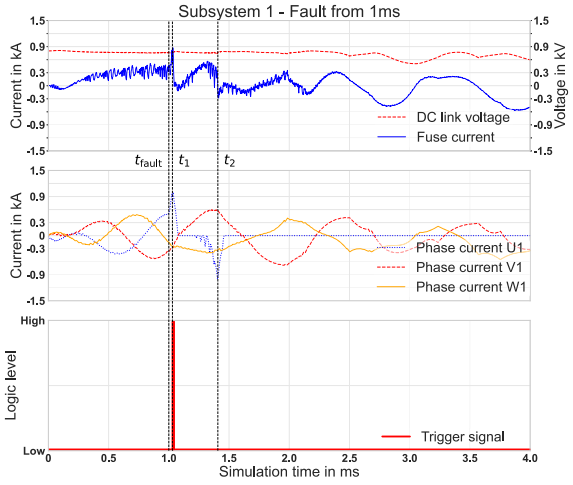


Fig. A.1. Measurement signals and output signals of the FDU for the subsystem 1 in the event of a short-circuit fault between the terminal of phase U in subsystem 1 and the star point of the subsystem 3 with active DESAT handling from 1 ms.

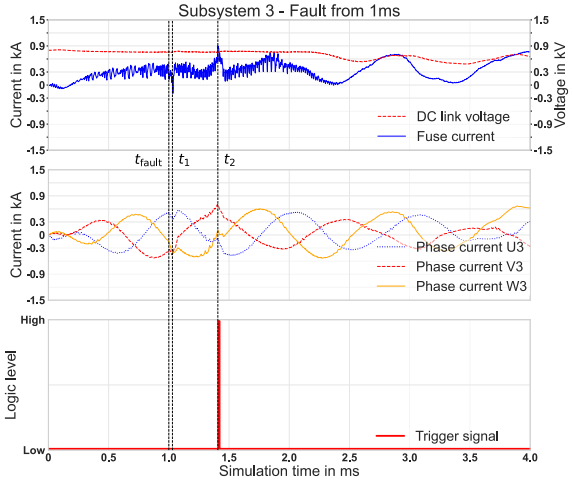


Fig. A.2. Measurement signals and output signals of the FDU for the subsystem 3 in the event of a short-circuit fault between the terminal of phase U in subsystem 1 and the star point of the subsystem 3 with active DESAT handling from 1 ms.

References

[1] F. Hilpert, C. Bentheimer, T. Mueller, B. Eckardt, Investigation of novel multi-phase field-Oriented drive inverter control with fail-operational capabilities for aircraft applications, in: PCIM Europe Digital Days 2021; International Exhibition and Conference for Power Electronics, Intelligent Motion, Renewable Energy and Energy Management, 2021, pp. 1–7.

[2] M. Villani, M. Tursini, G. Fabri, L. Castellini, Multi-phase fault tolerant drives for aircraft applications, in: Electrical Systems for Aircraft, Railway and Ship Propulsion, 2010, pp. 1–6. https://doi.org/10.1109/ESARS.2010.5665246

[3] M. Kozovsky, L. Buchta, P. Blaha, Compensation methods of interturn short-circuit faults in dual three-phase PMSM, in: IECON 2020 the 46th Annual Conference of the IEEE Industrial Electronics Society, 2020, pp. 4833–4838. https://doi.org/10.1109/IECON43393.2020.9254734

[4] M. Gleissner, M. Bakran, A real-life fuse design for a fault-tolerant motor inverter, in: Proceedings of the 18th European Conference on Power Electronics and Applications (EPE'16 ECCE Europe), 2016, pp. 1–11. https://doi.org/10.1109/EPE.2016.7695279

[5] T. Orlowska-Kowalska, M. Wolkiewicz, P. Pietrzak, M. Skowron, P. Ewert, G. Tarchala, M. Krzysztofiak, C.T. Kowalski, Fault diagnosis and fault-tolerant control of PMSM drives–state of the art and future challenges, IEEE Access 10 (2022). https://doi.org/10.1109/ACCESS.2022.3180153

[6] M.-C. Flynn, M. Sztykiel, C.E. Jones, P.J. Norman, G.M. Burt, P. Miller, M. Husband, Protection and fault management strategy maps for future electrical propulsion aircraft, IEEE Trans. Transp. Electrif. 5 (4) (2019) 1458–1469. https://doi.org/10.1109/TTE.2019.2940882

[7] P. Lell, D. Volm, Innovative safety concept to shutdown short circuit currents in battery systems up to 1000 v based on ultrafast pyrofuse technology, in: 2018 IEEE Holm Conference on Electrical Contacts, 2018, pp. 317–322. https://doi.org/10.1109/HOLM.2018.8611656

[8] D. Li, L. Qi, Energy based fuse modeling and simulation, in: 2013 IEEE Electric Ship Technologies Symposium (ESTS), 2013, pp. 487–492. https://doi.org/10.1109/ESTS.2013.6523781

[9] M. Koprivsek, Advanced solutions in over-current protection of HVDC circuit of battery-powered electric vehicle, in: PCIM Europe 2018; International Exhibition and Conference for Power Electronics, Intelligent Motion, Renewable Energy and Energy Management, 2018, pp. 1–4.

[10] R. Ouaida, J.F. de Palma, G. Gonthier, Hybrid protection based on pyroswitch and fuse technologies for DC applications, in: Symposium De Genie Electrique, 2016.

[11] T. Sakuraba, R. Ouaida, S. Chen, T. Chailloux, Evaluation of novel hybrid protection based on pyroswitch and fuse technologies, in: 2018 International Power Electronics Conference (IPEC-Niigata 2018 -ECCE Asia), 2018, pp. 2153–2157. https://doi.org/10.23919/IPEC.2018.8507793

[12] H. Bavishi, M. D'Arpino, P. Ramesh, Y. Guezennec, I. Colbert, Comparative analysis of protection systems for DC power distribution in electrified vehicles, in: SAE Technical Paper 2022-01-0135, 2022. https://doi.org/10.4271/2022-01-0135

[13] S. Altouq, K. Fong, P. Norman, G.M. Burt, Pyrofuse modeling for eVTOL aircraft DC protection, in: SAE Technical Paper 2021-01-0041, 2021. https://doi.org/10.4271/2021-01-0041

[14] K. Taraka, Pyro-fuse circuit, 2019, u.S. Patent: US20190123542A1.

[15] RTCA Committee, DO-178C: software considerations in airborne systems and equipment certification, 2011. RTCA DO-178C / EUROCAE ED-12C.

[16] M. Kozovsky, P. Blaha, Double three-phase PMSM structures for fail operational control, IFAC-PapersOnLine 52 (27) (2019). https://doi.org/https://doi.org/10.1016/j.ifacol.2019.12.733

[17] G. Choi, T.M. Jahns, Investigation of key factors influencing the response of permanent magnet synchronous machines to three-phase symmetrical short-circuit faults, IEEE Trans. Energy Convers. 31 (4) (2016) 1488–1497. https://doi.org/10.1109/TEC.2016.2594223

[18] G. Choi, T. Jahns, PM synchronous machine drive response to asymmetrical short-circuit faults, IEEE Trans. Ind. Appl. 52 (3) (2016) 2176–2185. https://doi.org/10.1109/TIA.2016.2518992

[19] G. Choi, T. Jahns, Investigation of key factors influencing the response of permanent magnet synchronous machines to three-phase symmetrical short-circuit faults, IEEE Trans. Energy Convers. 31 (4) (2016). https://doi.org/10.1109/TEC.2016.2594223

[20] B.A. Welchko, T. Jahns, W.L. Soong, J.M. Nagashima, IPM synchronous machine drive response to symmetrical and asymmetrical short circuit faults, IEEE Trans. Energy Convers. 18 (2) (2003). https://doi.org/10.1109/TEC.2003.811746

[21] J. Qazi, M. Ikeda, Failure Analysis of Capacitors and Inductors, ASM International, 2019, pp. 587–602. https://doi.org/10.31399/asm.tb.mfadr7.t91110587

[22] C. Boucharеb, N.-S. Mohamed-Said, PMSM model with phase-to-phase short-circuit and diagnosis by ESA and EPVA, Adv. Electr. Electron. Eng. 14 (2016). https://doi.org/10.15598/aeee.v14i5.1928

[23] L. Liu, K. Wang, L. Guo, J. Li, Analysis of inter-turn short circuit faults in dual three-phase PMSM for electromechanical actuator, IEEE Trans. Transp. Electrif. (2023). https://doi.org/10.1109/TTE.2023.3239632

[24] M. Kozovsky, L. Buchta, P. Blaha, Compensation methods of interturn short-circuit faults in dual three-phase PMSM, in: IECON 2020 the 46Th Annual Conference of the IEEE Industrial Electronics Society, 2020, pp. 4833–4838. https://doi.org/10.1109/IECON43393.2020.9254734

[25] L. Liu, K. Wang, L.L. Guo, J. Li, Analysis of inter-turn short circuit faults in dual three-phase PMSM for electromechanical actuator, IEEE Trans. Transp. Electrif. (2023) 1–1. https://doi.org/10.1109/TTE.2023.3239632

[26] A. Khlaief, M. Boussak, M. Gossa, Open phase faults detection in PMSM drives based on current signature analysis, in: The XIX International Conference on Electrical Machines - ICEM 2010, 2010, pp. 1–6. https://doi.org/10.1109/ICELMACH.2010.5607977

[27] M. Cheng, J. Hang, J. Zhang, Overview of fault diagnosis theory and method for permanent magnet machine, Chin. J. Electr. Eng. 1 (1) (2015) 21–36. https://doi.org/10.23919/CJEE.2015.7933135

[28] H. Li, Y. Qian, S. Asgarpoor, H. Sharif, Machine current sensor FDI strategy in PMSMs, IEEE Access 7 (2019). https://doi.org/10.1109/ACCESS.2019.2950429

[29] M. Albach, Elektrotechnik, Pearson Deutschland GmbH, Hallbergmoos, Germany, 1 edition, Hallbergmoos, Germany, 2011.

[30] K.W. Klontz, T. Miller, M. McGilp, H. Karmaker, P. Zhong, Short-circuit analysis of permanent-magnet generators, IEEE Trans. Ind. Appl. 47 (4) (2011). https://doi.org/10.1109/TIA.2011.2154370

[31] P. Xu, J.H. Feng, S.Y. Guo, S. Feng, W. Chu, Y. Ren, Z.Q. Zhu, Analysis of dual three-phase permanent-magnet synchronous machines with different angle displacements, IEEE Trans. Ind. Electron. 65 (3) (2018) 1941–1954. https://doi.org/10.1109/TIE.2017.2748035



Leonard Kuhn is with the Fraunhofer Institute for Integrated Systems and Device Technology, Department of Power Electronics, Group Aviation Electronics, Erlangen, 91058 Germany e-mail: leonard.kuhn@iisb.fraunhofer.de.He received his MSc in Mechatronic Engineering from the Friedrich-Alexander-Universität Erlangen-Nürnberg in 2023. As a researcher at Fraunhofer IISB he is working on electronic systems with the highest power densities and efficiencies. As a hardware developer for fault-tolerant and fault management systems in aviation applications, the focus is on all safety-critical aspects of aircraft powertrain components. The institute specializes in high-voltage powertrain development, including megawatt-scale and electrified aircraft systems. Expertise in lightweight, efficient power electronics with leading power density forms the foundation for his scientific work.



Markus Meindl received his MSc in Electrical Engineering from the Friedrich-Alexander-Universität Erlangen-Nürnberg in 2021 and is working to finalize his PhD in Electrical Engineering in 2025. Since July 2025, Markus has been appointed as the manager of the Fuel Cell and Hybrid System (FuCHS) research group at the Fraunhofer Institute for Integrated Systems and Device Technology (IISB). He is involved in several research and teaching projects at the Institute of Power Electronics at Friedrich-Alexander-Universität Erlangen-Nürnberg (FAU). During his PhD, he was the technical leader of the EU GENESIS project´s power electronics, electric drives, and on-ground energy supply development. He is involved in several other European Clean Aviation Projects. In the NEWBORN project, he serves as the Power Distribution System Lead and Power Line Lead for a 1 MW demonstrator setup of a hybrid-electric powertrain for future regional aircraft. His current research interests include sustainable hybrid-electric aircraft systems, power electronics for aircraft applications, improved utilization of electrical machines, on-ground energy supply systems for future airports, and transportation electrification in general.



Christian Bentheimer received his MSc in Electrical Engineering from the University of Stuttgart in 2017. Afterwards, he joined Fraunhofer IISB and was initially involved in designing and implementing integrated inverter drive systems for automotive and aviation applications. Since 2024, Christian has been appointed as the manager of the aviation electronics workgroup at Fraunhofer IISB. He specializes in developing wide band gap power electronic systems with the highest power densities and efficiencies. His team, consisting of experts from various disciplines, focuses on all aspects of the high-voltage "backbone" of electrified aircraft, utilizing the institutes' experiences from compact power electronic components to MW-scale energy distribution. Their current research is centered on the development of cryogenic inverter drive systems.